ments of $d\sigma/d\Omega$ at backward angles for $T_\pi > 180$ MeV, as well as of $a_{\pi d}$ and polarizations.

One of us (T.M.) thanks R. Vinh Mau and Institut de Physique Nucléaire, Orsay, for kind support, and the members of Institut de Physique Nucléaire, Lyon, for their warm hospitality.

[1]K. Gabathuler *et al.*, to be published; A. Stanovnik *et al.*, private communication; R. J. Holt *et al.*, Phys. Rev. Lett. 43, 1229 (1979); R. Frascaria *et al.*, Phys. Lett. 91B, 345 (1980).

[2]C. Richard-Serre *et al.*, Nucl. Phys. B20, 413 (1970); J. Spuller and D. Measday, Phys. Rev. D 12, 3550 (1975); C. Weddigen, Nucl. Phys. A312, 330 (1978).

[3]I. P. Auer *et al.*, Phys. Rev. Lett. 41, 354 (1978), and references therein.

[4]I. R. Afnan and A. W. Thomas, Phys. Rev. C 10, 109 (1974).

[5]T. Mizutani and D. S. Koltun, Ann. Phys. 109, 1 (1977); A. S. Rinat, Nucl. Phys. A287, 399 (1977); A. W. Thomas, *Theoretical Methods in Medium Energy and Heavy Ion Physics* (Plenum, New York, 1978).

[6]A. T. Stelbovics and M. Stingl, J. Phys. G 4, 1371, 1389 (1978).

[7]Y. Avishai and T. Mizutani, Nucl. Phys. A326, 352 (1979); A338, 377 (1980).

[8]A. W. Thomas and A. S. Rinat, Phys. Rev. C 20, 216 (1979).

[9]I. R. Afnan and B. Blankleider, to be published.

[10]W. M. Kloet and R. R. Silbar, Nucl. Phys. A338, 281, 317 (1980).

[11]Y. Avishai and T. Mizutani, to be published.

[12]T. Mizutani, Ph. D. thesis, University of Rochester (1975) (unpublished).

[13]A. S. Rinat, E. Hammel, Y. Starkand, and A. W. Thomas, Nucl. Phys. A329, 285 (1979).

[14]K. Schwarz, H. F. K. Zingl, and L. Mathelitsch, Phys. Lett. 83B, 297 (1979).

[15]N. Giraud, C. Fayard, and G. H. Lamot, Phys. Rev. C 21, 1959 (1980).

[16]Y. Avishai and T. Mizutani, to be published.

[17]M. Ida, Phys. Rev. 136, B1767 (1964).

[18]T. Mizutani, C. Fayard, and G. H. Lamot, to be published.

[19]H. Nielson and G. C. Oades, Nucl. Phys. B49, 573 (1972).

[20]R. Koch and E. Pietarinen, Nucl. Phys. A336, 331 (1980).

[21]J. Bailey *et al.*, Phys. Lett. 50B, 403 (1974).

[22]K. Kubodera, M. P. Locher, F. Myhrer, and A. W. Thomas, J. Phys. G 6, 171 (1980), and references therein.

Microscopic Description of Nucleon-Nucleus Total Reaction Cross Sections

N. J. DiGiacomo, R. M. DeVries, and J. C. Peng

Physics Division, Los Alamos Scientific Laboratory, Los Alamos, New Mexico 87545

(Received 4 February 1980; revised manuscript received 12 June 1980)

Microscopic calculations of the total reaction cross sections for protons on ^{12}C, ^{27}Al, ^{40}Ca, and ^{208}Pb, and neutrons on ^{27}Al and ^{208}Pb have been made, which provide for the first time an excellent description of the data for projectile energies from 15 MeV through 1 GeV. The calculations are based on the experimental nucleon-nucleon total cross sections and explicitly include the effects of the real nuclear potential, the Coulomb potential, Pauli blocking, and Fermi motion.

PACS numbers: 25.40.-h, 24.10.Dp

The total reaction cross section (σ_R) for the interaction of a nuclear projectile with a nucleus is perhaps the most basic nuclear reaction observable. Attempts to calculate this quantity[1-5] in a microscopic manner have generally begun with the experimental nucleon-nucleon scattering amplitudes or total cross sections and nuclear charge densities. Only above approximately 300 MeV can such calculations generally reproduce the data (e.g., Ref. 1). No calculations have been reported, however, which include the effects of the real nuclear potential, Pauli blocking, and Fermi motion. It is generally felt that all of the above effects are important for a realistic description of σ_R at lower energies.

In this Letter, we consider the energy and mass dependence of the nucleon-nucleus σ_R for which good quality data exist over a wide range of energy and mass. Extension can then hopefully be made to the more complicated nucleus-nucleus system. It will be interesting to see whether such calculations can reproduce the apparent[3,4] non-geometric behavior of nucleus-nucleus σ_R.

Viewing the nucleon-nucleus interaction semi-

classically, the transmission probability through the nucleus, for a given impact parameter b, is

$$T = \exp(-z/\lambda), \tag{1a}$$

where, for incident protons,

$$\lambda = (\rho \sigma_T^{pN})^{-1}. \tag{1b}$$

In Eq. 1, z is the path length through the nucleus, ρ is the average nuclear density and σ_T^{pN} is the isospin-averaged free proton-nucleon total cross section. The total reaction cross section is then

$$\sigma_R = 2\pi \int [1 - \exp(-z/\lambda)] b \, db. \tag{2}$$

Equation (2) can be made more realistic by allowing the Coulomb potential and the real nuclear potential to determine the path the projectile takes through the nucleus. The use of the real and Coulomb potentials to determine the path constitutes a first-order method of correcting for wave refraction effects in the scattering. For the calculation at hand, we consider only central potentials, i.e.,

$$V(r) = V_{\text{Coul}}(r) + V_{\text{real}}(r).$$

The Coulomb potential used for the proton-nucleus case is that due to a uniform charge distribution of radius $R_{\text{Coul}} = r_{\text{Coul}} A^{1/3}$ fm. We chose to use empirical determinations of the energy and mass dependence of the real volume integral to specify a Woods-Saxon form of $V_{\text{real}}(r)$ as a function of mass and energy. From 15 to 60 MeV the standard parametrizations available from the literature were used.[6-12] Above approximately 60 MeV the recent optical-model analysis of Nadasen *et al.*[13] was used. Their parametrization was extended to 1 GeV and found to be in good agreement with volume integrals determined from optical-model analyses of proton-nucleus elastic scattering at 800 MeV and 1 GeV.[14,15] Given the above considerations and the fact that our calculations become insensitive to the real potential above approximately 300 MeV, we feel that it is reasonable to extend the parametrization of Nadasen *et al.* to 300 MeV. This is approximately 100 MeV above the highest energy considered in their work.

The path through the nucleus is then simply the classical trajectory for a particle in a central force field.[16,17] Equation (2) is written as

$$\sigma_R(E) = 2\pi \int \{1 - \exp[-\chi(b,E)]\} b \, db, \tag{3}$$

where

$$\chi(b,E) = 2\pi \int_{r_{\min}}^{\infty} dr \{1 + (b/r)^2 [1 - V(r)/T - (b/r)^2]^{-1}\}^{1/2} [\rho_p(r) \sigma_T^{pp}(K(r)) + \rho_n(r) \sigma_T^{pn}(K(r))]. \tag{4}$$

In these expressions, r is the radial distance between the projectile and nuclear center, ds is an element of path length, T is the center of mass kinetic energy of the projectile, $\sigma_T^{pp}(K(r))$ $[\sigma_T^{pn}(K(r))]$ the local average effective proton-proton (neutron) total cross section (at the relative momentum of the projectile and the nucleus), and $r_{\min}$ is the distance of closest approach of the projectile for a given $V(r)$. The projectiles' path is symmetric about $r_{\min}$.[16]

Relativistic kinematics are used and the potential is treated in a relativistic manner.[16] The densities used are taken from the density-matrix-expansion (DME) calculations of Negele and Vautherin.[18] Their calculations yield not only realistic nuclear densities but also density-dependent Fermi momenta. This point will be elaborated upon later.

Now, at any point within the influence of $V(r)$, the relative momentum of the projectile and the nucleus is (nonrelativistically)

$$K(r) = (1/hc)(2mc^2)[T - V(r)]^{1/2}. \tag{5}$$

The proton-nucleon total cross sections are calculated for the relative momentum at each point along the trajectory. Thus, a net attractive (repulsive) potential causes the nucleon-nucleon collisions to occur at higher (lower) relative velocities.

We next consider the aforementioned Pauli-blocking and Fermi-motion effects within a degenerate-Fermi-gas model of the nucleus. This approach has been developed previously[19-21] in an analytic manner for specific functional parametrizations of the nucleon-nucleon total cross section. We perform the calculation numerically and input the free σ_T^{pn} and σ_T^{pp} from a six-point Gaussian interpolation of the existing data[22] above 20 MeV. Below 20 MeV we use a scattering-length parametrization.[23,24] The nucleons in the nucleus are assumed to be uniformly distributed in momentum space up to K_F. The projectile ($\vec{K}$) and a given nucleon in the nucleus ($\vec{K}_1$) have, before colliding, relative momentum $\vec{K} - \vec{K}_1$. After colliding they have relative momentum $\vec{K}' - \vec{K}_1'$. The scattering cross section of the nucleons is a function of their relative velocity, i.e., $|\vec{K}' - \vec{K}_1'|$

$=|\vec{K}-\vec{K}_1|=2k$. The Pauli principle requires that $|\vec{K}'|>K_F$ and $|\vec{K}_1'|>K_F$. The effect of this restriction is to limit the solid angle available to the scattered nucleons to some $\Omega'<4\pi$. The proton-proton effective total cross section, for example, in nuclear matter is then

$$\sigma_T^{pp}(\vec{K},K_F) = (\tfrac{4}{3}\pi K_F^3)^{-1}\int d^3K_1 \int d\Omega'(2k/K)\sigma_T^{pp}(k(r)). \quad (6)$$

Note that the Fermi motion is taken into consideration by the integration over all $\vec{K}_1$. The calculations of σ_T^{pp} are shown in Fig. 1.[25] When $|\vec{K}|<K_F$, there are no states available to the scattered nucleons; thus $\sigma_T^{pp}=0$.

The final ingredient in these calculations involves the density dependence of the Fermi momentum K_F. Initial calculations performed with use of electron scattering densities[26,27] and a local density relationship between $\rho(r)$ and K_F were encouraging, but overpredicted σ_R by as much as 25% at lower energies for light nuclei. Inclusion of a density-gradient correction[28] resulted in a slight improvement. Use of the densities and corresponding Fermi momenta calculated within the DME approach,[18] however, brought about excellent agreement with the data for all nuclei down to 20 MeV. The DME approach seems to be the most realistic means of providing $K_F(\rho(r))$. The DME densities are in good agreement with the experimental (electron-scattering) data except for a small disagreement for ^{12}C (rms charge radius = 2.59 fm, experiment = 2.46 fm). The neutron-nucleus calculations are performed in the same way, assuming $\sigma_T^{pp}=\sigma_T^{nn}$ and $\sigma_T^{pn}=\sigma_T^{np}$. There is, of course, no Coulomb term in the potential. Also, the appropriate neutron-nucleus optical potentials are used.

The simplest meaningful calculation which was performed considered a straight-line path (i.e., $V_{Real}=V_{Coul}=0$), and did not include Pauli blocking or Fermi motion. These results are shown, along with the data,[29] as dotted curves in Fig. 2. The solid lines in Fig. 2 are the results of calculations in which the real potential, Coulomb potential (where applicable), Pauli blocking, and Fermi motion were included. The calculations indicate that the Pauli blocking and Fermi motion decrease σ_R, while the real potential acts to offset this decrease. The tendency of the real po-

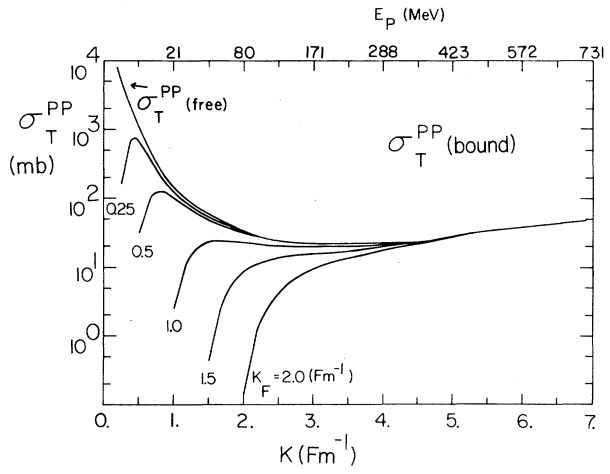

FIG. 1. The calculated proton-proton total cross section in nuclear matter [σ_T^{pp} (bound)] as a function of the relative momentum of the proton and the nucleus for representative values of K_F. Also shown is the free proton-proton total cross section [σ_T^{pp} (free)].

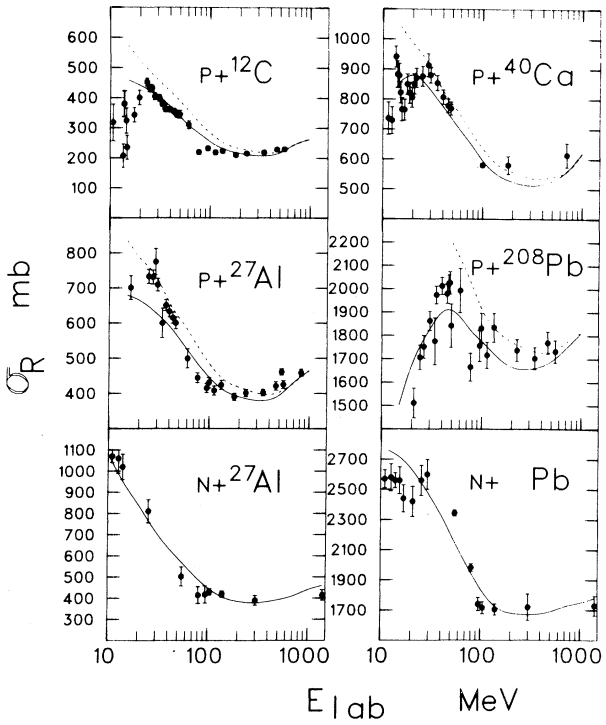

FIG. 2. The calculated proton-nucleus and neutron-nucleus total reaction cross section as a function of laboratory energy. Data shown were collected from Refs. 29(a)–29(r). The dotted curves are the results of calculations in which Eq. (3) was solved for a straight-line trajectory with no Fermi motion or Pauli blocking. The solid lines are the results of calculations in which the Coulomb (where applicable) and real nuclear potentials, Fermi motion, and Pauli blocking are included. The data shown for n + Pb include a number of isotopes.

tential to increase σ_R is due to the fact that the attractive real potential increases the relative velocity at which the nucleon-nucleon collisions occur. Indeed, a glance at Fig. 1 will verify that a small increase in K can increase σ_T^{pp} enormously. The similarity between the full and simple calculations implies that the heat potential roughly cancels the effects of Pauli blocking and Fermi motion. Also, the fact that the full calculations tend to the simple calculations at higher energies reflects the energy dependence of the real-potential, Pauli-blocking, and Fermi-motion effects.

It is interesting to note that the neutron-nucleus σ_R data do not reveal the energy-dependent oscillations seen in the neutron-nucleus total-cross-section data.[30] These oscillations are understood to occur in the elastic scattering.[31] Also, the difference between the proton and neutron σ_R at low energies (most notable for ^{208}Pb) reflects the importance of Coulomb potential.

In conclusion, we report for the first time a realistic microscopic calculation of nucleon-nucleus total reaction cross sections which agrees quite well with the data from 15 MeV through 1 GeV. The effects of the real nuclear potential, Coulomb potential, Pauli blocking, and Fermi motion are all seen to be important. It is indeed noteworthy that, by carefully including the physics known to be important at low energies, this Glauber-type model can describe σ_R over quite a wide energy range.

The authors would like to thank J. Ginocchio, J. Cramer, and G. Bertsch for useful discussions. We are especially grateful to John Negele for providing us with tabulations of densities and Fermi momenta for the nuclei considered in this work. This work was supported by the U. S. Department of Energy.

[1]L. Ray, Phys. Rev. C 20, 1857 (1979).
[2]D. Ernst, Phys. Rev. C 10, 896 (1979).
[3]R. DeVries and J. C. Peng, Phys. Rev. Lett. 43, 1373 (1979).
[4]R. DeVries and J. C. Peng, to be published.
[5]P. Schwaller *et al.*, Nucl. Phys. A316, 317 (1978).
[6]F. D. Becchetti and G. W. Greenlees, Phys. Rev. 181, 1190 (1969).
[7]W. T. H. Van Oers *et al.*, Phys. Rev. C 10, 307 (1974).
[8]C. M. Perey and F. G. Perey, Nucl. Data Tables 17, 1 (1976).
[9]W. T. H. Van Oers and H. Haw, Phys. Lett. 45B, 227 (1973).
[10]E. E. Gross *et al.*, Nucl. Phys. A102, 673 (1967).
[11]W. T. H. Van Oers, Phys. Rev. C 3, 1550 (1971).
[12]W. T. H. Van Oers and J. M. Cameron, Phys. Rev. 184, 1061 (1969).
[13]A. Nadasen *et al.*, Phys. Rev. C (to be published).
[14]L. Ray, private communication.
[15]M. Rayman, J. R. Shepard, and N. J. DiGiacomo, private communication.
[16]R. O. Newton, *Scattering Theory of Waves and Particles* (McGraw-Hill, New York, 1966).
[17]H. Goldstein, *Classical Mechanics* (Addison-Wesley, Cambridge, Massachusetts, 1950).
[18]J. Negele and D. Vautherin, Phys. Rev. C 5, 1472 (1971).
[19]M. L. Goldhaber, Phys. Rev. 74, 1269 (1948).
[20]E. Clementel and C. Villi, Nuovo Cimento 2, 176 (1955).
[21]K. Kikuchi and M. Kawai, *Nuclear Matter and Nuclear Reactions* (North-Holland, Amsterdam, 1968).
[22]W. Hess, Rev. Mod. Phys. 30, 365 (1958); O. Benary *et al.*, University of California Report No. UCRL-20000NM (unpublished).
[23]P. Marmier and E. Sheldon, *Physics of Nuclei and Particles* (Academic, New York, 1970), Vol. II, pp. 1053–1057.
[24]D. A. Saloner, C. Toepffer, and B. Fink, Nucl. Phys. A282, 131 (1977).
[25]Tabulations of σ_T^{pn} (bound), as well as σ_T^{pp} (bound) are available from the authors.
[26]L. Ray, W. Coker, and G. W. Hoffman, Phys. Rev. C 18, 2641 (1978).
[27]C. W. de Jager, H. DeVries, and C. DeVries, Nucl. Data Tables 14, 479 (1974).
[28]K. A. Bruckner *et al.*, Phys. Rev. 171, 1188 (1968).
[29]The $p + {}^{12}$C data can be found in references a, b, e, g, i, j, and k; the $p + {}^{27}$Al data in references d, e, f, g, h, i, j, k, and m; the $p + {}^{40}$Ca data in references b, c, j, n, and l; and the $p + {}^{208}$Pb data in references c, d, g, h, i, j, and k. The $n + {}^{27}$Al and n + Pb data can be found in references o, p, q, and r.
[a]B. D. Wilkins and G. Igo, Phys. Rev. 129, 2198 (1963).
[b]J. F. DiCello and G. Igo, Phys. Rev. C 2, 488 (1969).
[c]R. F. Carlson *et al.*, Phys. Rev. C 12, 1167 (1975).
[d]R. E. Pollack and G. Schrank, Phys. Rev. 140, B575 (1965).
[e]W. F. McGill *et al.*, Phys. Rev. C 10, 2237 (1974).
[f]M. Q. Makino *et al.*, Nucl. Phys. 50, 145 (1964).
[g]J. J. Menet *et al.*, Phys. Rev. C 4, 1114 (1971).
[h]T. J. Gooding, Nucl. Phys. 12, 241 (1959).
[i]R. Golonskie and K. Straugh, Nucl. Phys. 29, 474 (1962).
[j]P. Kirby and T. Link, Can. J. Phys. 44, 1847 (1966).
[k]P. U. Renberg *et al.*, Nucl. Phys. A183, 81 (1972).
[l]B. D. Anderson *et al.*, Phys. Rev. C 19, 905 (1979).
[m]D. Bugg *et al.*, Phys. Rev. 146, 980 (1966).
[n]A. Johansson *et al.*, Ark. Fys. 19, 527 (1961).
[o]T. Coor *et al.*, Phys. Rev. 98, 1369 (1955).
[p]R. G. P. Voss and R. Wilson, Proc. Roy. Soc. London, Ser. A 236, 41 (1956).

[q]J. B. Marion and J. L. Fowler, *Fast Neutron Physics, Part II*, Interscience, New York, 1963.
[r]W. P. Ball, University of California Report No. UCRL-1938, 1952 (unpublished).
[30]D. Hughes, *Neutron Cross Sections* (Pergamon Press, New York, 1957), p. 66.
[31]A. Bohr and B. Mottelson, *Nuclear Structure* (Benjamin, New York, 1969), p. 165.

Observation of the Infrared Spectrum of H_3^+

Takeshi Oka
Herzberg Institute of Astrophysics, National Research Council of Canada, Ottawa, Ontario K1A 0R6, Canada
(Received 10 June 1980)

The infrared ν_2 band of H_3^+ has been observed. A direct infrared absorption method combining a liquid-nitrogen–cooled multiple-reflection discharge cell and a difference-frequency laser system has been used for the detection. Fifteen absorption lines have been measured in the region of 2950–2450 cm^{-1} and assigned. This is the first spectroscopic detection of this fundamental molecular ion in any spectral range.

PACS numbers: 33.20.Ea, 35.20.Pa, 36.90.+f

Since its discovery by Thomson,[1] the triatomic hydrogen molecular ion H_3^+ has been well known to mass spectroscopists. Because of the efficient exothermic reaction[2] $H_2 + H_2^+ \rightarrow H_3^+ + H$ and its large dissociation energy, H_3^+ is the most abundant ion in a hydrogen discharge. It is also the simplest polyatomic system, and is an important catalyst in interstellar ion chemistry.[3] However, there has previously been no spectroscopic information on this fundamental ion. The recent major advances in our knowledge of this ion have been (a) the detailed *ab initio* calculation by Carney and Porter,[4] (b) the confirmation of the equilateral-triangle structure by the novel method of foil-induced dissociation by Gaillard *et al.*,[5] and (c) the observation of Rydberg-state emission spectra of neutral H_3 and D_3 by Herzberg.[6] In this paper, I report the first observation of the spectrum of H_3^+. The transitions observed are rovibrational transitions in the active degenerate ν_2 infrared-band.

A direct infrared absorption method combining a multiple-reflection discharge cell and a frequency-tunable infrared source was chosen as the detection method. The multiple-reflection discharge cell was 2 m long and was cooled with liquid nitrogen, as was done by Woods and his collaborators[7] for their microwave detection of CO^+, HCO^+, and HNN^+. For the tunable infrared source, a difference-frequency laser system developed by Pine[8] was used. Mixing radiation from an Ar laser (ν_A) and that from a dye laser (ν_D) in a temperature-controlled $LiNbO_3$ crystal, we obtained an infrared radiation source with the power of a few microwatts whose frequency ($\nu_A - \nu_D$) was tunable over the range of 4400–2400 cm^{-1}. The frequency of the infrared radiation was modulated by modulating the frequency of the Ar laser with an amplitude of ~400 MHz and a frequency of 2.5 kHz. The signal was processed ($1f$ detection) through a phase-sensitive detector. The overall sensitivity for the search was $\sim 1.5 \times 10^{-2}$ and, with a path length of 32 m, the minimum detectable absorption coefficient was $\sim 4 \times 10^{-6}$ cm^{-1}. This sensitivity was checked by observing the weak $v = 1 \leftarrow v = 0$ quadrupole spectrum[9] of D_2.

The direct absorption method is much less sensitive than the ingenious ion-beam laser-resonance method of Wing and his collaborators,[10] who were successful in detecting the infrared spectra of HD^+ and HHe^+, and the laser magnetic resonance method of Saykally and Evenson,[11] who detected HBr^+. However, it makes it possible to cover a wide range of the infrared region and this coverage was essential in the detection of H_3^+ because the spectrum extends over a region of ~500 cm^{-1} and the estimated accuracy of the theoretical prediction[12] was ~50 cm^{-1}.

The density of H_3^+ in the hydrogen discharge (current density ~60 mA/cm^2, pressure ~1 Torr) is estimated to be $n \sim 3 \times 10^{10}/cm^3$ from the electron drift velocity[13] ($v_d \sim 10^7$ cm/sec) and the fraction of H_3^+ among other positive ions, $f \gtrsim 0.75$, reported by Saporochenko.[14] The translational and rotational temperature of H_3^+ is estimated to be not much higher than 200 K from the energy dissipation (~1 kW) and the thermal conductivity of the

